Solution X-ray Scattering Data Show Structural Differences between Yeast and Vertebrate Calmodulin: Implications for Structure/Function†

Hidenori Yoshino,*,‡ Yoshinobu Izumi,§ Kazuyoshi Sakai,§ Hikaru Takezawa,§ Isao Matsuura,||,⊥ Hironobu Maekawa,|| and Michio Yazawa||

Department of Chemistry, Sapporo Medical University, S-1, W17, Chuo-ku Sapporo 060, Japan, Macromolecular Research Laboratory, Faculty of Engineering, Yamagata University, 4-3-16 Jo-nan Yonezawa 992, Japan, Department of Chemistry, Faculty of Science, Hokkaido University, N-10, W-8, Kita-ku Sapporo 060, Japan

Received September 6, 1995; Revised Manuscript Received December 5, 1995⊗

ABSTRACT: We present here the first evidence, obtained by the use of solution X-ray scattering, of the solution structure of yeast calmodulin, a poor activator of vertebrate enzymes. The radius of gyration of yeast calmodulin decreased from 21.1 to 19.9 Å when excess Ca^{2+} ions were added. The profiles of the pair-distribution function suggested that yeast calmodulin without Ca^{2+} has a dumbbell-like shape which changes toward a rather asymmetric globular shape, from its dumbbell shape, by the binding of Ca^{2+}. In the presence of a calmodulin binding peptide such as MLCK-22 (a synthetic peptide corresponding to residues 577−598 of skeletal myosin light chain kinase), the radius of gyration of yeast calmodulin decreased by 1.6 Å, and the molecular shape of it estimated from the profile of the pair-distribution function was globular but less compact than that of vertebrate calmodulin. These results for the structure of yeast calmodulin complexed with Ca^{2+} and with Ca^{2+}−peptides are quite different from those of vertebrate calmodulin. Thus, the functional differences between yeast and vertebrate calmodulin which we reported previously [Matsuura, I., et al. (1993) *J. Biol. Chem. 268,* 13267−13273] have been interpreted on the basis of the structural differences between them. Moreover, the structural studies on chimeric proteins of chicken and yeast calmodulin suggest that Ca^{2+} binding at site IV is essential to form the full active dumbbell structure, which is characteristic of vertebrate-type calmodulin.

Calmodulin (CaM)[1] is a protein of small size which appears in all eukaryotic cells and regulates many significant cellular function as a versatile decoder of Ca^{2+} signals. The structure of Ca^{2+}-saturated vertebrate CaM in the crystalline state resembles a dumbbell in which the N-terminal half (N-lobe) is connected to the C-terminal half (C-lobe) by a central linker-helix of approximately eight turns (Babu et al., 1985, 1988; Kretsinger et al., 1986; Chattopadhyaya et al., 1992). A pair of Ca^{2+} binding sites is located in each of the lobes (Ca^{2+}-binding sites I and II in the N-lobe, and III and IV in the C-lobe). The Ca^{2+} binding affinity of the C-lobe is higher than that of the N-lobe (Yazawa et al., 1987). Much effort has so far been devoted to the study of structure−function relationships of CaM. The major questions are the functional significance of the dumbbell shape and the functional differences among the four Ca^{2+} binding sites.

Table 1: Functional Properties of CaMs[a]

		activation parameters			
		PDE		MLCK	
CaMs	Ca^{2+} binding numbers	K_{act} (nM)	V_{max} (%)	K_{act} (nM)	V_{max} (%)
scallop CaM	4	1.6	100	2.2	100
YCM0	3	1200	110	4200	2
C4Y	3	220	110	220	60
C4Y140E	4	1.7	100	1.7	110

[a] The data are taken from our previous report (Matsuura et al., 1993). The activity obtained at saturating scallop CaM (vertebrate-type CaM) with Ca^{2+} was defined as 100%. K_{act} is the concentration of CaMs required for half-maximal activation.

The primary structure of CaMs is extremely conservative, and homology of the sequence is greater than 90% among vertebrates and invertebrates including marine invertebrates such as scallop (Toda et al., 1985). The primary structure of CaM from baker's yeast (*Saccharomyces cerevisiae*), however, shares only 60% identity with vertebrate CaM, and functionally, yeast CaM does not bind Ca^{2+} at site IV and is a poor activator of vertebrate enzymes (Luan et al., 1987; Ohya et al., 1987; Davis et al., 1986; Matsuura et al., 1991).

To explore the functional role of Ca^{2+} binding to the site IV and/or C-lobe, we have produced recombinant yeast CaM (YCM0) and chimeric proteins of chicken and yeast CaM. C4Y consists of Ala^{1}−Ile^{130} of chicken (including Ca^{2+} binding sites I, II, and III) and Asp^{131}−Lys^{148} of yeast (including site IV) CaM, and C4Y140E is produced by a single substitution of Glu for Gln^{140} in the C4Y. Table 1 summarizes our previous results on the activation profiles of phosphodiesterase (PDE) and myosin light chain kinase

† This work was supported by Proposal 93G225 from Photon Factory Advisory Committee, Tsukuba, Japan. H.Y. is supported in part by the Akiyama Foundation, Japan, and M.Y. is supported in part by a Grant-in-Aid for Scientific Research on Priority Area 05209201 from the Ministry of Education, Science and Culture of Japan.

* To whom correspondence should be addressed.
‡ Sapporo Medical University.
§ Yamagata University.
|| Hokkaido University.
⊥ Present address: Department of Biochemistry, Hong Kong University of Science & Technology, Clear Water Bay, Kowloon, Hong Kong.

⊗ Abstract published in *Advance ACS Abstracts,* February 1, 1996.

[1] Abbreviations: MLCK-22, synthetic peptide corresponding to residues 577−598 of skeletal myosin light chain kinase; CaM, calmodulin; PDE, phosphodiesterase; MLCK, myosin light chain kinase; SOXS, solution X-ray scattering; Rg, radius of gyration; MP, mastoparan.

0006-2960/96/0435-2388$12.00/0

(MLCK) by these proteins (Matsuura et al., 1993). Both YCM0 and C4Y bind only three moles of Ca^{2+} because of a defect in the Ca^{2+} binding at site IV, and have low affinities to both PDE and MLCK (compare the K_{act} values in Table 1). These results indicate that YCM0 and C4Y have a low-affinity structure, though scallop CaM, which is functionally classified as vertebrate-type CaM, and C4Y140E have a high-affinity structure. Moreover, YCM0 activated PDE but not MLCK (see the V_{max} values in Table 1).

A solution X-ray scattering method that can be useful for studying the structure of CaM in solution was originally demonstrated by Seaton and co-workers (1985) and then by ourselves and others (see below). We demonstrated that the solution structure of vertebrate CaM in the presence of Ca^{2+} had a elongated bilobed shape that could be regarded as basically a dumbbell (Matsushima et al., 1989; Yoshino et al., 1989). Further SOXS analyses comparing the solution and crystal structures of CaM in detail suggested that the distance between the two lobes of CaM in solution was smaller than that in the crystal structure, thus indicating flexibility at the linker region of CaM molecule (Heidorn & Trewhella, 1988). Indeed, the considerable flexibility at the center part of the linker region (residues 78−81) has been proved by an NMR study on CaM in solution (Ikura et al., 1991). These findings indicate that the solution structure of CaM is not exactly the same as the crystal structure, though CaM in solution still remains a fairly elongated bilobed structure. In addition, the flexibility implies a possibility of structural divergence of CaM, in which the distance between the two lobes of CaM in solution varies from one molecule to another. Since SOXS measurements provide information on the time-averaged structure rather than a single "snapshot" structure, of the scattering molecules, it is difficult to show a unique structure by the SOXS method.

While the SOXS method is limited by its lower resolution as compared to X-ray crystallography, a significant advantage of this method is that structural analysis can be performed under desirable conditions, for instance, under varying pH, intermediate Ca^{2+} concentrations, or in the presence of various CaM binding peptides. A series of SOXS data for vertebrate CaM with CaM binding peptides indicated that a drastic shape transition of vertebrate CaM from a dumbbell to a compact globular structure was induced by the binding of small peptides such as mastoparan (Yoshino et al. 1989), melittin (Kataoka et al., 1989), MLCK-22 related peptide (Heidorn et al., 1989), and other peptides [reviewed by Trewhella (1992)]. Since these peptides, including mastoparan (Malencik & Anderson, 1983), are thought to be the model peptides of the CaM binding domain in CaM-dependent enzymes, it is conceivable that the shape transition of CaM may play a key role in the activation mechanism of target enzymes.

We do not as yet know the structure of yeast CaM. Therefore, our interests have focused on the solution structure of yeast CaM alone and complexed with model peptides in order to identify the low-affinity and less active structure. As model peptides, we chose mastoparan and MLCK-22 in this report. Wasp venom mastoparan binds to brain CaM with high affinity (the dissociation constant is about 0.3 μM) and is a competitive inhibitor for the binding of MLCK to brain CaM (Malencik & Anderson, 1983) suggesting that CaM in a complex with mastoparan can be an appropriate model for CaM bound to target protein. For that reason, we have accumulated considerable structural evidence of brain CaM complexed with masotoparan (Matsushima et al., 1989; Yoshino et al., 1989; Izumi et al., 1992). However, mastoparan is not a natural target binding domain of CaM. Thus we used here MLCK-22 as a natural target peptide in order to confirm the results obtained with mastoparan.

MATERIALS AND METHODS

Materials. Mastoparan (synthesized product) having the sequence INLKALAALAKKIL was purchased from the Peptide Institute Co. (Osaka, Japan) and used without further purification. The MLCK-22 peptide having the sequence KRRWKKNFIAVSAANRFKKISS was synthesized on an Applied Biosystem Model 431 A Peptide synthesizer using the general procedure. The crude peptide dissolved in water was filtrated (Millipore filter, 0.45 μm) and purified by a Sephadex G25 (Medium) (Pharmacia LKB) column (1.5 × 30 cm) chromatography. The purified MLCK-22 peptide was freeze-dried and kept at −80 °C after weighing. The peptides were dissolved in water and used after adjustment of pH of the solution.

Bovine brain CaM was prepared and purified by the exactly same methods as previously described (Yoshino et al., 1993). Recombinant yeast CaM, YCM0, and chimeric proteins of chicken and yeast CaM were produced by exactly the same procedure of protein engineering as previously described in detail (Matsuura et al., 1993). The concentration of proteins was determined by the method of Lowry et al. (1951).

SOXS Measurements. The SOXS data for proteins were obtained using the BL-10C instrument, which was installed at the Photon Factory in the National Laboratory for High Energy Physics at Tsukuba, Japan. The basic medium used for the SOXS measurements was 50 mM Tris-HCl, pH 7.6, and 120 mM NaCl; the molar ratios of Ca^{2+} denoted in this paper were the added molar ratios of Ca^{2+} per mol of protein, and Ca^{2+}-free proteins were placed in 1 mM EDTA. The temperature of the scattering experiment was kept at 25 °C by circulating water through the cell holder. The volume of the measuring cell was 70 μL.

The radius of gyration (R_g) was calculated from the scattering data in the very small angle region by the Guinier method (Guinier & Fournet, 1955), in which R_g is written as a function of SOXS intensity, $[I(s)]$, as $\log[I(s)] = \log[I(0)] - [4\pi^2/3]R_g^2s^2$. In this report, s is the reciprocal coordinate, $2\sin\theta/\lambda$ (2θ, the scattering angles; λ, the wavelength of X-ray used, 1.448 Å). The pair-distribution function, $P(r)$, is calculated by a direct Fourier transformation: $P(r) = 8\pi \int I(s)(sr) \sin(2\pi sr)\, ds$, where I is the scattering intensity and s is the reciprocal coordinate as mentioned above. Other details of the methods of data analyses were described elsewhere (Matsushima et al., 1989; Yoshino et al., 1989).

RESULTS

The protein concentration dependence of the R_g values of CaMs is shown in Figure 1, and the intrinsic R_g values obtained by extrapolation to infinite dilution of the curves in Figure 1 are summarized in Table 2. It is noted that Ca^{2+} binding to YCM0 causes a 1.2 Å decrease in the intrinsic R_g value, whereas Ca^{2+} binding to brain CaM causes a 0.6

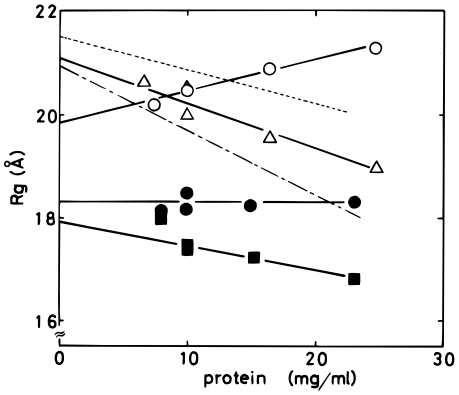

FIGURE 1: Protein concentration dependence of R_g values for YCM0 and brain CaM. The R_g values were obtained in 50 mM Tris-HCl (pH 7.6) and 120 mM NaCl at 25 °C. The circles and triangles are the R_g values of YCM0 in the presence of 1 mM EDTA (Δ), in the presence of a 5-fold molar excess of Ca^{2+} without the peptide (○), and with equimolar MLCK-22 (●). The squares are the R_g values of brain CaM in the presence of a 5-fold molar excess of Ca^{2+} and equimolar MLCK-22 (■). Shown are our previous results obtained with brain CaM (Matsushima et al., 1989) in the presence of a 5-fold molar excess of Ca^{2+} (- - -), and in the presence of 1 mM EDTA (− − −) at the same buffer conditions as described above.

Å increase in it. Consequently, the intrinsic R_g value of YCM0−Ca^{2+} is 1.6 Å smaller than that of brain CaM−Ca^{2+}.

At every machine time for SOXS measurements, we have always checked carefully the Guinier plots and R_g values of fresh brain CaM at a fixed concentration of 10 mg/mL as standard. The R_g values of standard brain CaM in these 4 years, under the same medium conditions as that in this report, were 20.0 ± 0.41 Å ($n = 7$) for CaM without Ca^{2+}, 21.2 ± 0.36 Å ($n = 10$) for CaM−5Ca^{2+}, and 18.1 ± 0.26 Å ($n = 5$) for CaM−5Ca^{2+}−MP, respectively. the R_g values of YCM0 obtained at a fixed concentration of 10 mg/mL using two separate preparations were 20.3 ± 0.42 ($n = 2$) Å for YCM0 without Ca^{2+}, 20.3 ± 0.21 Å ($n = 3$) for YCM0 with 5Ca^{2+}, and 19.2 ± 0.10 Å ($n = 2$) for YCM0−5Ca^{2+}−MP, respectively. Consequently, the reliability of the R_g values for the CaMs in our experiments should be within ±0.4 Å, indicating the significance among the differences of R_g values between brain CaM and YCM0 described above. The intrinsic R_g values of brain CaM with Ca^{2+} reported from several laboratories are basically consistent, while those values without Ca^{2+} are slightly different from laboratory to laboratory. An interpretation of the discrepancy is provided in our previous paper (Yoshino et al., 1993).

As shown in Figure 1, the slope of YCM0−Ca^{2+} is quite different from that of brain CaM−Ca^{2+}. The positive slope does not mean simple aggregation of YCM0−Ca^{2+}, because the Guinier plots of YCM0−Ca^{2+} have no upward curvature at very low scattering angles (data not shown). In addition, the intensity of forward scatter at infinite dilution of YCM0s, which brought evidence for the molecular weight of scattering particles, indicated no significant difference between YCM0 without Ca^{2+} and YCM0−5Ca^{2+}, suggesting no considerable aggregation of YCM0−5Ca^{2+}. Since the slope of the plot in Figure 1 reveals the interparticle interference among protein molecules (Izumi et al., 1992), the molecular state of YCM0−Ca^{2+} would be considerably different from that of brain CaM−Ca^{2+}. In the absence of Ca^{2+}, however, the R_g value of YCM0 is close to that of brain CaM, and the slope of YCM0 shown in Figure 1 resembles that of brain CaM, indicating a similar molecular size and molecular state between them.

In the presence of CaM binding peptides such as mastoparan or MLCK-22, the R_g value of YCM0−Ca^{2+} decreased, indicating that confirmational changes toward the contracted form were induced by binding of the peptides, though the decrease by 0.7 Å with mastoparan and that by 1.6 Å with MLCK-22 observed in YCM0 are smaller (by more than 3.6 Å) than those of brain CaM (Figure 1 and Table 2). The R_g values of C4Y and C4Y140E are also decreased by the presence of the peptides, though the values are obtained at fixed protein concentrations (Table 2). The complex of YCM0−Ca^{2+}−MLCK−22 shows no significant concentration dependence, while the complex of brain CaM−Ca^{2+}-MLCK−22 has a moderately negative slope, suggesting slightly different molecular states for these two molecules (Figure 1).

The R_g values of YCM0 were changed by the presence of model peptides such as mastoparan or MLCK-22 in a Ca^{2+}-dependent manner, and the changes were almost complete upon the addition of 2 mol Ca^{2+} per mol of YCM0 as shown in Figure 2. As was predicted from the result in Figure 1, the R_g value of YCM0 at a protein concentration of about 10 mg/mL without the peptides scarcely changed irrespective of Ca^{2+} concentration (data not shown). The R_g values of YCM0 in EDTA with MLCK-22 were always slightly higher than those without the peptide. Further experiments would be needed to explain the differences.

The pair-distance distribution function [$P(r)$] is sensitive to the shape of the scattering particle (Trewhella, 1992). The calculated $P(r)$ profile of a dumbbell-shaped object has two distinct maxima corresponding to the diameter of each lobe and the distance between the lobes. $P(r)$ approaches zero at d_{max}, which provides an estimate of the maximum linear dimension of the scattering particle. The $P(r)$ profile of brain CaM with Ca^{2+} (Figure 3A, ●) displays two distinct maxima, the first at 21 Å, and the second at around 45 Å, though the shape of the latter is a hump rather than a peak because of its lower intensity. The d_{max} is 69 Å. These values approximate those estimated from crystal structure. Moreover, the behavior of $P(r)$ profile is characteristic of a dumbbell-shaped object. Consequently, it is reasonable to consider that the time-averaged structure of brain CaM−Ca^{2+} in solution has basically a dumbbell shape. The $P(r)$ profile should therefore be a relevant criterion for the molecular shape of yeast type CaMs.

In the absence of Ca^{2+}, all $P(r)$ profiles of proteins have maxima at around 20 Å and clear humps at around 45 Å (Figure 3A−D, ○). The solution structure of these proteins in the Ca^{2+}-free form is a dumbbell shape in which the two lobes, of diameters of about 20 Å, are connected at a distance of about 45 Å. The R_g values of these proteins support that conclusion (Table 2).

In the Ca^{2+}-saturated condition, the $P(r)$ profiles of YCM0 and C4Y have maxima at 23 and 22 Å with less pronounced humps at around 45 Å (Figure 3B and D, ●). These are quite different from the findings for brain CaM, suggesting that the solution structures of YCM0 and C4Y less resemble dumbbells than nondumbbells when Ca^{2+} has bound at sites I, II, and III. The $P(r)$ profile of Ca^{2+}-saturated C4Y140E (Figure 3C, ●), however, has a maximum at 21 Å and a clear hump at around 45 Å, indicating a dumbbell-like shape similar to brain CaM.

Table 2: Structural Parameters of CaMs Obtained by SOXS[a]

	Guinier analysis [R_g (Å)]				$P(r)$ analysis[b] [d_{max} (Å)]			
CaMs	$-Ca^{2+}$	$5Ca^{2+}$	$5Ca^{2+}$ + MP	$5Ca^{2+}$ + MLCK-22	$-Ca^{2+}$	$5Ca^{2+}$	$5Ca^{2+}$ + MP	$5Ca^{2+}$ + MLCK-22
brain CaM	20.9	21.5	17.8	17.9	66	69	55	53
YCM0	21.1	19.9	19.2	18.3	~80	~85	~73	~65
C4Y	20.6	19.5	19.0	18.0	67	~72	57	58
C4Y140E	20.5	20.2	18.3	18.2	67	67	55	55

[a] The values of $-Ca^{2+}$ and $5Ca^{2+}$ were obtained in 1 mM EDTA and in the presence of a 5-fold molar excess of Ca^{2+} to proteins, respectively. The values with MP (mastoparan) and MLCK-22 were obtained in the presence of equimolar peptides. The SOXS measurements were performed in 50 mM Tris-HCl (pH 7.6) and 120 mM NaCl at 25 °C. The R_g values of brain CaM and YCMO except for YCM0−$5Ca^{2+}$−MP are the intrinsic R_g values as described in the text, and those of YCM0−$5Ca^{2+}$−MP, C4Y, and C4Y140E were obtained at a fixed protein concentration of about 10 mg/mL. The reliability of the R_g values in our experiments is described in the text. [b] The d_{max} values for YCM0 and C4Y−Ca^{2+} are only rough estimations [noted by the approximation symbols (~)], due to the extreme tailing and small wens on their $P(r)$ profiles, as described in the Discussion section. The deviation of d_{max} values of brain CaM in these 2 years were 67 ± 0.8 Å (n = 4) for CaM without Ca^{2+}, 69 ± 0.6 Å (n = 4) for CaM−$5Ca^{2+}$, and 55 ± 1.0 Å (n = 4) for CaM−$5Ca^{2+}$−MP, respectively (n = the number of separate SOXS measurements performed).

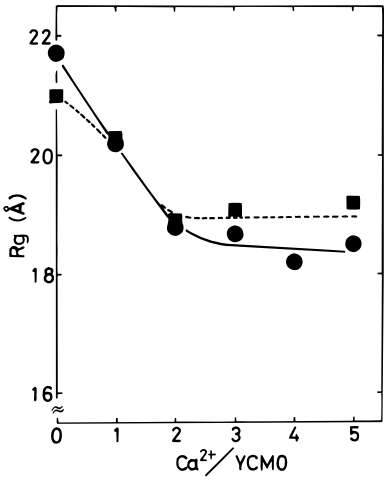

FIGURE 2: Calcium-dependent change in R_g of YCM0 in the presence of MLCK-22 or mastoparan. The R_g values were obtained with 10.0 mg/mL YCM0 with equimolar MLCK-22 (●) or mastoparan (■) in the buffer solution of 50 mM Tris-HCl (pH 7.6) and 120 mM NaCl at 25 °C.

The structures of the proteins in a complex with the model peptides were analyzed using mastoparan. The $P(r)$ profile of the complex of brain CaM−Ca^{2+} with mastoparan displays a single peak at 24 Å without any hump (Figure 3A, ▲). The R_g and d_{max} values of the complex are considerably smaller than those of uncomplexed CaM−Ca^{2+} (Table 2). These SOXS data indicate a compact globular shape for the complex of brain CaM−Ca^{2+} with mastoparan (Yoshino et al., 1989). The $P(r)$ profile of C4Y140E−Ca^{2+} complexed with mastoparan is exactly like that of brain CaM (Figure 3C, ▲), indicating a compact globular structure in the complex following a major shape transition, just as for brain CaM. The complex of C4Y with Ca^{2+}/mastoparan has a d_{max} and $P(r)$ profile similar to those of brain CaM (Figure 3D, ▲), which also indicates a globular shape for this complex. On the other hand, the $P(r)$ profile of the complex of YCM0 with Ca^{2+}/mastoparan behaves quite differently from that of brain CaM, particularly at higher r values (Figure 3B, ▲). The $P(r)$ profile, with its extreme tailing, and the large d_{max} value of the YCM0−Ca^{2+}−mastoparan complex relative to those of brain CaM indicate that the complex has a largely asymmetric globular shape rather than a compact globular shape.

As shown in Figure 4, the $P(r)$ profiles of YCM0 in the presence of mastoparan and also of MLCK-22 change depending on the Ca^{2+} concentration. The changes in $P(r)$ profiles, as well as the R_g change, for both peptides were complete upon the addition of 2 mol Ca^{2+} per mol of YCM0. The $P(r)$ profiles for Ca^{2+}-saturated YCM0−MLCK-22 complex are similar to those for YCM0−Ca^{2+}−mastoparan, whose structure is assumed to be less compact as described above.

DISCUSSION

Since CaM can express a biological function only when it binds Ca^{2+} ions, it is important to compare the structure of yeast CaM−Ca^{2+} with that of brain CaM−Ca^{2+} to implicate the functional differences between them. All the structural parameters of YCM0−Ca^{2+} including the intrinsic R_g value, the slope of the plot in Figure 1, and the $P(r)$ profile shown here are largely different from that of brain CaM−Ca^{2+}. Consequently, the solution structure of YCM0−Ca^{2+} is quite different from that of brain CaM−Ca^{2+}. Based on the structural parameters, particularly the $P(r)$ profile, it is reasonable to consider an asymmetrical globular-like structure for YCM0−Ca^{2+} rather than a dumbbell shape. It should be noted, however, that the Ca^{2+}-free form of YCM0 has a dumbbell-like structure similar to brain CaM.

The $P(r)$ profiles of YCM0 and C4Y with Ca^{2+} (panels B and D in Figure 3) show extreme tailing and small wens at higher r values, causing difficulties in the estimation of d_{max} values (noted by the ripple mark in Table 2). It is hard to explain those behaviors of the $P(r)$ profiles exactly. While speculative, our assumption is that the C-terminus region, including about 20 amino acid residues, of yeast-type CaMs has a slack structure, producing considerable asymmetry in the yeast type CaM−Ca^{2+} molecule.

Taking together the results of SOXS and the functional properties of those proteins shown in Table 1, it is reasonable to conclude as follows. The asymmetric globular-like shape of yeast-type CaM would correspond to the low-affinity structure and the dumbbell shape of vertebrate-type CaM would correspond to the high-affinity structure. Ca^{2+} binding to site IV is essential to form the high-affinity dumbbell structure. These conclusions are consistent with our previous report, in which Ca^{2+} binding to the C-lobe was sufficient to stabilize brain CaM in a dumbbell shape and induce stable complexes with CaM binding peptides (Yoshino et al., 1993). Only the dumbbell-shaped CaM can fully open up its own binding sites to various target enzymes. In contrast, in YCM0 or C4Y, the binding sites might be partially hidden in the asymmetric globular-like protein molecule, and/or the presumably flexible tail region at the C-terminus inhibits the binding of target enzymes, even if some binding sites are

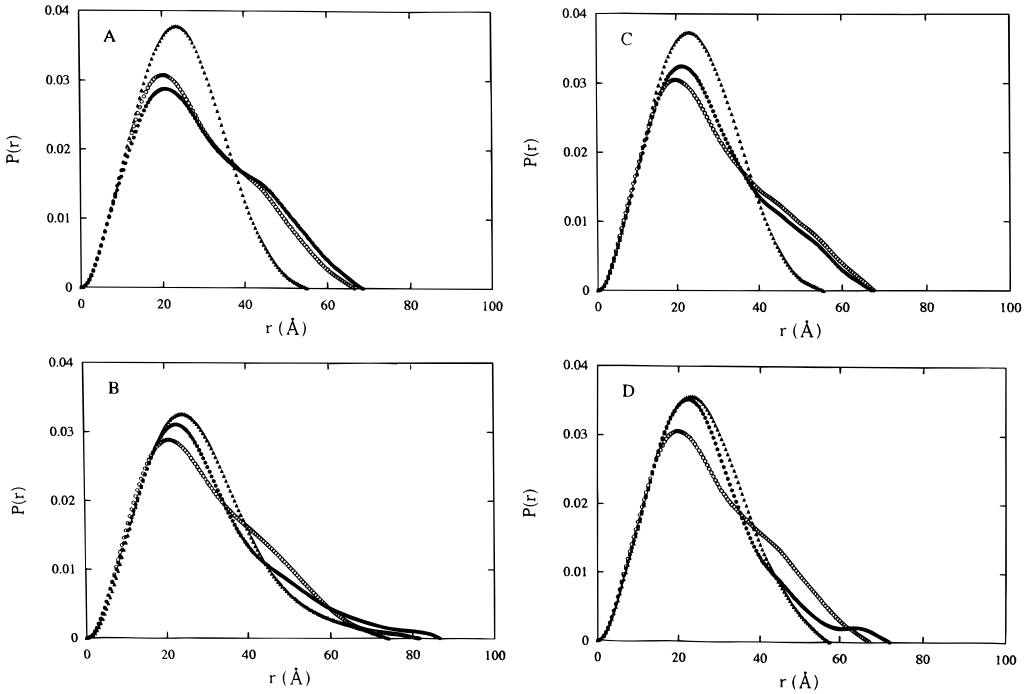

FIGURE 3: Pair distribution function, $P(r)$, of various CaMs. Panels A, B, C, and D are the $P(r)$ profiles of brain CaM, YCM0, C4Y140E, and C4Y, respectively. The SOXS of the CaMs (~10 mg/mL) were measured at 25 °C in 50 mM Tris-HCl (pH 7.6) and 120 mM NaCl, containing 1 mM EDTA (○), a 5-fold molar excess of Ca^{2+} to CaM (●), and a 5-fold molar excess of Ca^{2+} with an equimolar concentration of mastoparan to CaM (▲), respectively.

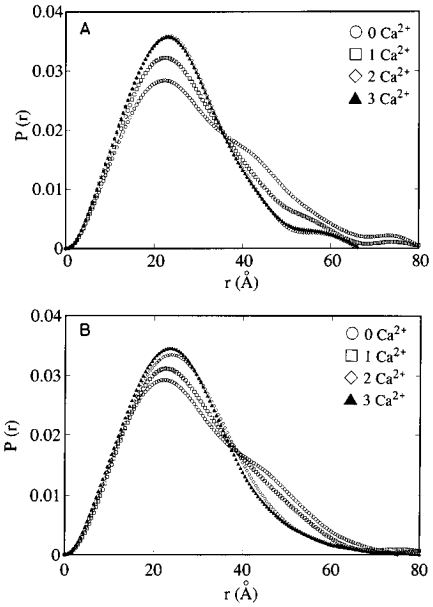

FIGURE 4: The calcium-dependent change in the $P(r)$ profile of YCM0 in the presence of MLCK-22 or mastoparan. The $P(r)$ profiles were obtained at 10 mg/mL YCM0 with equimolar MLCK-22 (panel A) or mastoparan (panel B) in a buffer solution of 50 mM Tris-HCl (pH 7.6) and 120 mM NaCl at 25 °C. The added molar ratio of Ca^{2+} per mole of YCM0 for each profile is denoted in the figure, and the $P(r)$ profiles of 0 Ca^{2+} in both panels are obtained in the presence of 1 mM EDTA.

induced on YCM0 and C4Y by Ca^{2+} binding to sites I, II, and III.

In the presence of equimolar mastoparan with excess Ca^{2+} and brain CaM, the R_g value decreases by 3.6 Å and the $P(r)$ profile displays a single peak without any hump (Figure 3A). These SOXS data have been interpreted as indicating that CaM undergoes a transition to a compact globular shape upon complex formation (Yoshino et al., 1989). A similar result was obtained with MLCK-22 (Yoshino et al., unpublished data) and the MLCK-22 related peptide (Heidorn et al., 1989). Recently, NMR and studies of the crystal structure of vertebrate CaM complexed with model peptides have confirmed the globular shape. In the complexes, the flexible region of the central linker, including about 10 amino acids, formed a loop or an expanded conformation going from a helix, which allowed the peptide to emerge between the two lobes of CaM by bending at the flexible region (Ikura et al., 1992; Meador et al., 1992, 1993). The idea of bending structure was predicted by the model studies (Persechini & Kretsinger; 1988; Ktretsinger, 1992).

Since the shape transition of CaM might play an essential role in activation of the target enzymes (Yoshino et al., 1993), it is interesting to elucidate the solution structure of yeast CaM in the complex with CaM binding model peptides. Without Ca^{2+}, all CaMs assume a dumbbell-like shape, whereas the binding of Ca^{2+}/mastoparan induces a shape transition in all CaMs (Figure 3). Consequently, when a CaM binds a target enzyme, depending on the Ca^{2+} occupancy, it may change shape and thereby influence the local structure of the target enzyme. The structural effects might be enough to activate PDE, since V_{max} values of PDE by all CaMs are almost the same (Table 1).

Brain CaM, C4Y140E, and C4Y, whose structures are roughly compact-globular after the binding of Ca^{2+}/mastoparan, activate MLCK, whereas YCM0, which fails to form a compact globular shape in the complex with Ca^{2+}/mastoparan, cannot activate MLCK (Table 1). The less compact structure of YCM0 with Ca^{2+}/MLCK-22, similar to that of YCM0 with Ca^{2+}/mastoparan, has been confirmed as shown in panel A of Figure 4. Presumably, new functional sites that are required to activate MLCK approach each other when CaM metamorphoses into a compact globular structure (Su et al., 1994) but might be relatively

distant in the inactive complex of YCM0 with Ca^{2+}/MLCK. A restricted orientation of the two lobes fixed by a specific interaction between each lobe and MLCK would be necessary in order for new functional sites to form. The orientation of the two lobes in the complex of C4Y with Ca^{2+}−mastoparan might be slightly different from that of brain CaM because C4Y had a pronounced tailing at higher r values of the $P(r)$ profile (Figure 3D, ●) suggesting a less compact structure than brain CaM had (note the area covered under the $P(r)$ curves with the abscissa at higher values than 40 Å in Figure 3). Therefore, C4Y shows an intermediate V_{max} value to MLCK. Possibly, the structure of vertebrate-type N-lobe is basically required to form the new functional site via the specific interaction mentioned above, because C4Y has the vertebrate type N-lobe whereas YCM0 has the yeast type N-lobe. Since C4Y140E, which has the vertebrate type N-lobe and has capability of Ca^{2+} binding at site IV, expresses full activity, the Ca^{2+} binding at site IV may help to form the complete new functional site which is perfected only in the compact globular structure as revealed in the $P(r)$ profile of brain type CaM (▲ in panels A and C of Figure 3). The Ca^{2+} binding at site IV is essential not only to form a high-affinity structure but also to rearrange the two lobes of CaM to form the new functional sites.

It is noted that SOXS studies have proved an elongated structure of vertebrate CaM in the complex with phK-13 peptide (a synthetic peptide corresponding to residues 301−326 of phosphorylase kinase) (Trewhella et al., 1990), and with C20W peptide (a synthetic peptide corresponding to residues 1100−1119 of plasma membrane Ca^{2+} pump (Kataoka et al., 1991). The binding of peptide does not always cause CaM to become a compact globular shape even in vertebrate CaM. The precise structural requirements, including the size, for a peptide to induce a compact globular shape in brain CaM are still unclear (Yoshino et al., 1993).

The dissociation constants (K_d) for Ca^{2+} bound to YCM0, C4Y, and C4Y140E are lower than 10 μM (Matsuura et al., 1992), and all the K_d values shift toward the submicromolar range or less in the presence of MLCK-22 (unpublished data) or mastoparan (Yazawa et al., 1987). Therefore, the binding molar ratios of Ca^{2+} per mol of protein in this study can be estimated from the value of the added molar ratios of Ca^{2+} per mol of protein, because the concentrations of Ca^{2+} used in our experiments are higher than the submillimolar range.

In the presence of mastoparan or MLCK-22, the shape change of YCM0 saturated by the binding of 2 mol Ca^{2+} per mol of YCM0, is revealed by the R_g values and $P(r)$ profiles (Figures 2 and 4). These results indicate that at least 1 mol of Ca^{2+} binding to N-lobe of YCM0 is required for the shape transition. However, we do not know individual Ca^{2+} binding affinity for N- or C-lobe and/or sites I, II, and III of YCM0. It is therefore difficult to argue which Ca^{2+} bindings are essential for the shape transition of YCM0, and also which Ca^{2+} bindings are required to bind the peptides on YCM0.

ACKNOWLEDGMENT

We thank Dr. Katsumi Kobayashi for help in the measurements of SOXS.

REFERENCES

Babu, Y. S., Sack, J. S., Greenhough, T. J., Bugg, C. E., Means, A. R., & Cook, W. J. (1985) *Nature 315*, 37−40.

Babu, Y. S., Bugg, C. E., & Cook, W. J. (1988) *J. Mol. Biol. 204*, 191−204.

Chattopadhyaya, R., Meador, W. E., Means, A. R., & Quiocho, F. A. (1992) *J. Mol. Biol. 228*, 1177−1192.

Davis, T. N., Urdea, M. S., Masiarz, F. R., & Thorner, J. (1986) *Cell 47*, 423−431.

Guinier, A., & Fournet, G. (1955) in *Small-Angle Scattering of X-rays*, John Wiley & Sons, New York.

Heidorn, D. B., & Trewhella, J. (1988) *Biochemistry 27*, 909−915.

Heidorn, D. B., Seeger, P. A., Rokop, S. E., Blumenthal, D. K., Means, A. R., Crespi, H., & Trewhella, J. (1989) *Biochemistry 28*, 6757−6764.

Ikura, M., Spera, S., Barbato, G., Kay, L. E., Krinks, M., & Bax, A. (1991) *Biochemistry 30*, 9216−9228.

Ikura, M., Clore, G. M., Gronenborn, A. M., Zhu, G., Klee, C. B., & Bax, A. (1992) *Science 256*, 632−638.

Izumi, Y., Wakita, M., Yoshino, H., & Matsushima, N. (1992) *Biochemistry 31*, 12266−12271.

Kataoka, M., Head, J. F., Seaton, B. A., & Engelman, D. M. (1989) *Proc. Natl. Acad. Sci. U.S.A. 86*, 6944−6948.

Kataoka, M., Head, J. F., Vorherr, T., Krebs, J., & Carafoli, E. (1991) *Biochemistry 30*, 6247−6251.

Kretsinger, R. H. (1992) *Science 258*, 50−51.

Kretsinger, R. H., Rudnick, S. E., & Weissman, L. J. (1986) *J. Inorg. Biochem. 28*, 289−302.

Lowry, O. H., Rosebrough, N. J., Farr, A. L., & Randall, R. J. (1951) *J. Biol. Chem.* **193**, 265−275.

Luan, Y., Matsuura, I., Yazawa, M., Nakamura, T., & Yagi, K. (1987) *J. Biochem. (Tokyo) 102*, 1531−1537.

Malencik, D. A., & Anderson, S. R. (1983) *Biochem. Biophys. Res. Commun. 114*, 50−56.

Matsushima, N., Izumi, Y., Matsuo, T., Yoshino, H., Ueki, T., & Miyake, Y. (1989) *J. Biochem. (Tokyo) 105*, 883−887.

Matsuura, I., Ishihara, K., Nakai, Y., Yazawa, M., & Yagi, K. (1991) *J. Biochem. (Tokyo) 109*, 190−197.

Matsuura, I., Kimura, E., Tai, K., & Yazawa, M. (1993) *J. Biol. Chem. 268*, 13267−13273.

Meador, W. E., Means, A. R., & Quiocho, F. A. (1992) *Science 257*, 1251−1255.

Meador, W. E., Means, A. R., & Quiocho, F. A. (1993) *Science 262*, 1718−1721.

Ohya, Y., Uno, I., Ishikawa, T., & Anraku, Y. (1987) *Eur. J. Biochem. 168*, 13−19.

Persechini, A., & Kretsinger, R. H. (1988) *J. Cardiovasc. Pharmacol. 12 (Suppl. 5)*, s1−s12.

Seaton, B. A., Head, J. F., Engelman, D. M., & Richard, F. M. (1985) *Biochemistry 24*, 6740−6743.

Su, Z., Fan, D., & George, S. E. (1994) *J. Biol. Chem. 269*, 16761−16765.

Toda, H., Yazawa, M., Sakiyama, F., & Yagi, K. (1985) *J. Biochem. (Tokyo) 98*, 833−842.

Trewhella, J. (1992) *Cell Calcium 13*, 377−390.

Trewhella, J., Blumenthal, D. K., Rokop, S. E. & Seeger, P. A. (1990) *Biochemistry 29*, 9316−9324.

Yazawa, M., Ikura, M., Hikichi, K., Ying, L., & Yagi, K. (1987) *J. Biol. Chem. 262*, 10951−10954.

Yoshino, H., Minari, O., Matsushima, N., Ueki, T., Miyake, Y., Matsuo, T., & Izumi, Y. (1989) *J. Biol. Chem. 264*, 19706−19709.

Yoshino, H., Wakita, M., & Izumi, Y. (1993) *J. Biol. Chem. 268*, 12123−12128.

BI952121V